Intermetallics 17 (2009) 25–31

Contents lists available at ScienceDirect

Intermetallics

journal homepage: www.elsevier.com/locate/intermet

Spin-glass-like behaviour in the ternary $U_3Fe_{4+x}Al_{12-x}$ uranium–iron aluminide

A.P. Gonçalves [a,*], J.C. Waerenborgh [a], P. Gaczyński [a], H. Noël [b], O. Tougait [b]

[a] Departamento de Química, Instituto Tecnológico e Nuclear/CFMC-UL, P-2686-953 Sacavém, Portugal
[b] Sciences Chimiques de Rennes, Laboratoire de Chimie du Solide et Matériaux. UMR CNRS 6226, Université de Rennes 1, Avenue de Général Leclerc, 35042 Rennes, France

ARTICLE INFO

Article history:
Received 25 February 2008
Received in revised form 6 June 2008
Accepted 12 September 2008
Available online 2 November 2008

Keywords:
A. Aluminides, miscellaneous
A. Magnetic intermetallics
B. Crystal chemistry of intermetallics
B. Magnetic properties
F. Diffraction

ABSTRACT

The $U_3Fe_{4+x}Al_{12-x}$ ($0 < x < 0.5$) intermetallic was prepared by arc melting, followed by annealing at 850 °C. This compound crystallizes in the hexagonal $Gd_3Ru_4Al_{12}$-type structure (e.g. $P6_3/mmc$), with room temperature parameters $a = 8.7516(3)$ Å and $c = 9.2653(4)$ Å for $x = 0$. The structure is characterized by planar layers of M3Al4 (M = Gd, U), containing *M* atoms in a triangular arrangement and forming a distorted Kagomé net. Magnetic measurements revealed a spin-glass-type behaviour with a freezing temperature, $T_f = 7.9$ K. The magnitude of the frequency shift of the freezing temperature is ≈0.03 and a Vogel–Fulcher law is followed with values typical for a spin-glass. ^{57}Fe Mössbauer data show that there is no freezing of the iron magnetic moments directions below T_f, indicating that the origin of the spin-glass-like behaviour is related to topological frustration of the uranium moments.

1. Introduction

Macroscopic spin-glass-like behaviour has been observed in many magnetic systems, ranging from solutions of magnetic transition metals dissolved in a noble metal host (canonical spin glasses) to superparamagnets. The magnetic interactions in spin glasses can be due to long-range RKKY indirect exchange interactions, as observed in the canonical spin-glass systems, or short range interactions, as seen in materials where ferromagnetic and antiferromagnetic interactions coexist (Ising spin-glass systems). Other types of spin glasses that have recently attracted an increasing interest of researchers are systems with an ordered crystal structure (or with only "non-magnetic atom disorder") where a geometrical frustration due to the lattice configuration dominates [1].

The recently performed phase equilibrium study of the U–Fe–Al ternary system at $T = 850$ °C has revealed a very rich system, with the formation of seven ternary intermetallic phases, together with three ternary extensions of the uranium binary phases [2]. The ternary phases form in the restricted region with a $(Fe + Al)/U \geq 2$ composition ratio. All of them crystallize in a previously known crystal structure type: UFe_2Al_{10} ($YbFe_2Al_{10}$-type), $U_2Fe_{3.6}Al_{13.4}$ (Th_2Ni_{17}-type), $U_2Fe_{12}Al_5$ (Th_2Ni_{17}-type), $UFe_{1+x}Al_{1-x}$ ($MgZn_2$-type); $U_2Fe_{17-x}Al_x$ (Th_2Zn_{17}-type); UFe_xAl_{12-x} ($ThMn_{12}$-type), and $U_3Fe_{4+x}Al_{12-x}$ ($Gd_3Ru_4Al_{12}$-type). As expected, their low temperature physical properties depend on their atomic ratios, and more particularly on the uranium and iron contents, as well as on their structure type. For instance, the tetragonal $ThMn_{12}$ ferromagnetic-type alloy UFe_xAl_{12-x} exhibits a continuous decrease of the Curie temperature from 363 K to 25 K with decrease in the iron content from $x = 7$ to $x = 3$ [3,4], and in the aluminium-rich region the other ternary aluminide, UFe_2Al_{10}, does not show any magnetic ordering down to 5 K [5].

From the new phases identified in the phase equilibrium study, $U_3Fe_{4+x}Al_{12-x}$ is of special interest: it crystallizes in the $Gd_3Ru_4Al_{12}$ structure type [6], with the uranium atoms forming a distorted Kagomé net, qualifying it as a good candidate for a spin-glass-like behaviour system due to geometrical frustration. Moreover, spin-glass-like behaviour was recently evidenced in the isotypic cobalt compound $U_3Co_{4+x}Al_{12-x}$ [7,8].

In this paper we present a detailed structural study of the $U_3Fe_4Al_{12}$ compound, together with magnetization, AC-susceptibility and ^{57}Fe Mössbauer spectroscopy investigation on a 1U:1Fe:3Al nominal composition sample, containing the $U_3Fe_{4+x}Al_{12-x}$ compound as the major phase.

2. Experimental

The elements used in the synthesis were uranium ingots (depleted uranium platelets 99.8%, Merck, surface cleaned in diluted HNO_3 before use), iron and aluminium pieces (99.9%, Strem). The samples were first prepared by arc melting the appropriate amounts of the three elements. The buttons were turned over and melted two more times in order to ensure

* Corresponding author. Tel.: +351 219946182; fax: +351 219946185.
E-mail address: apg@itn.pt (A.P. Gonçalves).

0966-9795/$ – see front matter © 2008 Elsevier Ltd. All rights reserved.
doi:10.1016/j.intermet.2008.09.003

complete homogenization. The alloys were then wrapped in tantalum foil and annealed at 850 °C for two weeks in silica tubes sealed under vacuum.

Powder X-ray diffraction spectra were collected at room temperature, from fine powdered samples, on a Panalytical X'Pert PRO diffractometer equipped with a back monochromator and using Cu Kα radiation, with a 2θ-step size of 0.03° from 10° to 115°. The identification of the phases was made by comparing the observed experimental powder patterns and those calculated using the program PowderCell [9]. The Rietveld analysis was done applying the FullProf program [10] and assuming the $Gd_3Ru_4Al_{12}$ structure type [6]. An experimentally determined $K_{\alpha1}/K_{\alpha2}$ intensities ratio of 0.5 and a factor $\cos(\theta) = 0.7998$ for the monochromator polarization correction were used in the Rietveld refinement. Two cell parameters, a zero-point, the extinction factor, the scale factor, a Pseudo-Voigt shape, a background (adjusted with a polynomial function), eight position parameters (x for two 6 h and one 12 k, y for two 6 h and one 12 k, and z for 12 k and 4f positions) and six occupation factors, in a total of 22 parameters, were refined. The crystallographic and experimental data of the structural determination are listed in Table 1.

The microstructure of the samples and composition of the phases were studied on polished surfaces using the JEOL-JSM 6400 scanning electron microscope (SEM) equipped with an Oxford Link-Isis Si/Li device for energy dispersive X-ray spectroscopy (EDS). Quantitative data, allowing a good determination of the homogeneity ranges, were obtained by using the stoichiometric binary compounds UAl_2, UAl_3 and UFe_2 as reference standards. For magnetization and ^{57}Fe Mössbauer measurements, the sample with 1U:3Fe:3Al nominal composition was used, since the only impurity phase in this sample is the non-magnetic $UAl_{2-x}Fe_x$ (see below).

AC-susceptibility and magnetization measurements were carried out on fixed powdered samples in the 2–300 K temperature range, using a MagLab system (Oxford Instruments) or a SQUID (Quantum Design) magnetometer. Both components of the AC-susceptibility, $\chi = \chi' + i\chi''$, were recorded using frequencies between 30 and 10,000 Hz and excitation fields between 1 and 500 Oe. Magnetization versus temperature measurements were performed after zero-field cooling (ZFC) and field cooling (FC) between room temperature and 1.8 K, and under fields up to 2 T. The variation of the magnetization as a function of the magnetic field was studied up to 7 T at $T = 1.8$ K.

Mössbauer spectra were collected at room temperature, $T = 25$ and 4 K in transmission mode using a conventional constant-acceleration spectrometer and a 25 mCi ^{57}Co source in a Rh matrix. The velocity scale was calibrated using α-Fe foil. The absorber was obtained by pressing the powdered sample (5 mg of natural Fe/cm^2) into a perspex holder. Isomer shifts (IS) are given relative to metallic α-Fe at room temperature. The 25 K spectrum was collected using a liquid He flow cryostat while the 4 K spectrum was obtained with the sample immersed in liquid He in a bath cryostat. The spectra were fitted to Lorentzian lines using a non-linear least-squares method [11]. The relative areas and widths of both peaks in a quadrupole doublet were kept equal during the refinement.

Table 1
Parameters for data recording and structural refinements of the $U_3Fe_4Al_{12}$ sample

Compound	$U_3Fe_4Al_{12}$
Space group	$P6_3/mmc$
Cell parameters, Å	$a = 8.7350(6)$
	$c = 9.2478(6)$
Volume, Å^3	611.1(1)
Wavelength, Å	Cu Kα
Data range, °2θ	10–115
Counting step, °2θ	0.03
Counting time, s	20
Number of reflections	404/2
Number of refined parameters	22
Zero point, °2θ	0.062(2)
Asymmetry parameters	−0.081(9)
	0.029(2)
	0.070(3)
	−0.23(2)
Preferred orientation [001]	0.059(5)
Halfwidth parameters	
U	0.14(1)
V	−0.04(1)
W	0.020(2)
Rietveld reliability factors, %	
R_P	16.8
R_{WP}	14.7
χ^2	8.4
R_B	6.37
R_F	5.38

3. Crystal structure identification and stoichiometry

In the course of the ternary phase diagram investigation, several samples were prepared at, and around the atomic ratio U:Fe:Al = 20:20:60. The set of the main diffraction peaks of the X-ray powder patterns could be unambiguously indexed according to the hexagonal $Gd_3Ru_4Al_{12}$ structure type (space group $P6_3/mmc$), indicating the formation of the $U_3Fe_4Al_{12}$ compound. In fact, this structure type is known to generate non-stoichiometric phases, as found for the prototype itself, reported with the $Gd_3Ru_{4+x}Al_{12-x}$ formula [6]. The EDS quantitative analysis of samples with different compositions around the U:Fe:Al = 16:21:63 atomic ratio (which corresponds to the ideal $U_3Fe_4Al_{12}$ compound) indicated that this phase forms within a homogeneity range $U_3Fe_{4+x}Al_{12-x}$ with $0 < x < 0.5$, as can be seen on the ternary plot [2]. It is well known that iron and aluminium can substitute one another up to a rather large extent in most of the ternary phases, and particularly those deriving from the $ThMn_{12}$ and the $MgZn_2$ structure types [12]. Moreover, the binary Al–Fe system itself forms successive substitution phases extending from Fe to FeAl.

As indicated on the phase diagram [2], $U_3Fe_{4+x}Al_{12-x}$ is in equilibrium with five other intermetallic phases, namely: $UAl_{2-x}Fe_x$ ($MgCu_2$ type), $UAl_{3-x}Fe_x$ ($AuCu_3$ type) $U_2Fe_{3.6}Al_{13.4}$ (Th_2Ni_{17}-type); UFe_xAl_{12-x} ($ThMn_{12}$-type), and $UFe_{1+x}Al_{1-x}$ ($MgZn_2$-type). So, even after long time annealing and due to its peritectic formation, it was not possible to prepare a pure $U_3Fe_{4+x}Al_{12-x}$ sample, free from one or two of these surrounding phases.

However, due to the presence of only very small amounts (<1% vol) of UFe_xAl_{12-x} and $UAl_{2-x}Fe_x$ (that can be detected by SEM/EDS analysis and in the magnetic measurements), it was decided to perform the $U_3Fe_{4+x}Al_{12-x}$ crystal structure Rietveld refinement from the powder X-ray data obtained on a 3U:4Fe:12Al nominal composition sample. In a preliminary refinement was considered the presence of the UFe_4Al_8 and UAl_2 compounds in the sample, but the low weight fractions obtained for these two phases (<0.5%) lead us not to consider them in the last refinements (Fig. 1). The lattice parameters refinement gave $a = 8.7350(6)$ Å and $c = 9.2478(6)$ Å, close to those previously observed for the isostructural $U_3Co_{4.55}Al_{11.45}$ alloy [7]. The last least-squares structure refinement converged to final $R_{Bragg} = 0.0637$ and $R_F = 0.0538$, confirming that the 3U:4Fe:12Al sample is mainly formed by a phase which has the $Gd_3Ru_4Al_{12}$ structure type. The refined atomic positions and occupation factors are presented in Table 2.

4. Structural features

Although it was not possible to find any single crystal suitable for X-ray diffraction, and in spite of the existence of small amounts

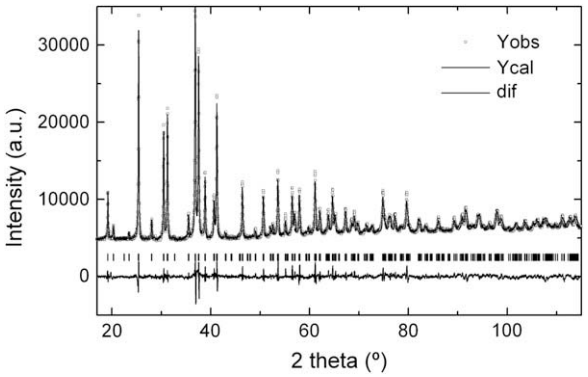

Fig. 1. Experimental powder diffraction profile for the 3U:4Fe:12Al nominal composition sample (squares) and calculated pattern for $U_3Fe_4Al_{12}$ (continuous line). The lower profile gives the difference between the experimental and calculated data and the tick lines indicate the position of the reflections.

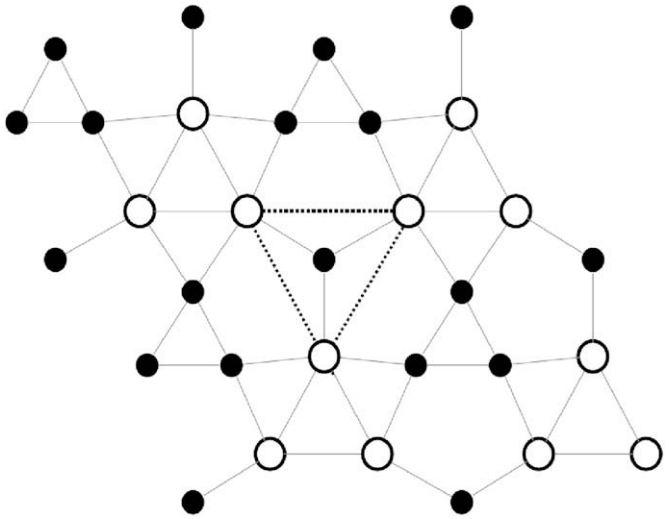

Fig. 2. Projection of the U3Al4 layers on the *ab* plane. White circles represent the uranium atoms and the black ones represent aluminium; the uranium atoms are located at the apexes of small and larger triangles, forming a distorted Kagomé net.

of impurity phases in the sample used in the Rietveld analysis (which affect the quality of the data), it is reasonable to assume that the reduced atomic parameters obtained in the refinement are close to the real ones. This is indeed corroborated by the similarity with the internal parameters found for the single crystal structure refinement of the cobalt-based compound $U_3Co_{4+x}Al_{12-x}$ [7]. However, in the present work and after considering the isotropic thermal parameters fixed with reasonable values, the refined occupation factors converge to values slightly higher than unity. The magnitude of the occupation factors did not allow a proper refinement of the aluminium substitution by iron in any atomic position. Nevertheless, the higher values observed for the 12k, 6h and 4f sites suggest that, if there is a substitution, it should be in one of these positions, most likely in the 6h position, as in the case of the cobalt compound [7].

As previously described for other isotypic compounds [6,7,13], the $U_3Fe_{4+x}Al_{12-x}$ crystal structure consists of U3Al4 layers alternating with FeAl layers along the hexagonal *c* axis. Fig. 2 shows that in the U3Al4 layers, the uranium atoms are located at the apexes of small and larger triangles, thus forming a distorted Kagomé net. The number of nearest neighbours and their interatomic distances, obtained in the X-ray refinement for the different crystallographic positions, are listed in Table 3. In $U_3Fe_4Al_{12}$, the shortest U–U distances are 3.54(1) Å, slightly higher than the Hill critical distance. Furthermore, only one of the Fe atoms (Fe1) belong to the uranium coordination sphere, located at 3.267 Å, considerably above the sum of their metallic radii (1.26 Å for iron, 1.43 Å for aluminium and 1.53 Å for uranium, for a coordination number of 12 [14]). This probably results in a weak hybridization of the 5*f* electrons of uranium with 3*d* and/or 4*s* electrons of the Fe1 atoms and, as a consequence, in a possible significant magnetic moment on both atoms. It is also interesting to notice the unusually short interatomic distances between the Al4(2b) and Fe2(2a) sites, 2.306(4) Å, indicating very strong interactions between these two atoms.

In the Mössbauer spectrum taken at 300 K (Fig. 3) three resolved peaks are observed. Considering that two different crystallographic sites are occupied by iron in the $U_3Fe_4Al_{12}$ structure, this spectrum was analyzed considering two quadrupole doublets. The best fit is obtained for the parameters summarized in Table 4. The estimated relative areas, *I*, are consistent with the full occupation of 2*a* and 6*g* crystallographic sites in excellent agreement with the Rietveld refinement of powder X-ray diffraction data. The doublet with lower I, attributed to site 2*a*, also has the lower quadrupole splitting, QS, which is consistent with the higher symmetry of this Wyckoff position. QS of this contribution is lower than the widths, Γ, of the individual lines of the doublet thus explaining why they are unresolved. The 25 K spectrum may be fitted by the same model. The refined QS, Γ and *I* values (Table 4) are within the experimental accuracy identical to those at 300 K. The increase in IS between room temperature and 25 K is explained by the second-order Doppler shift.

Table 2
Atomic coordinates and isotropic thermal parameters for the $U_3Fe_4Al_{12}$ compound

Atom	Wyckoff position	*x*	*y*	*z*	O.F.	B_{iso}, Å^2
U	6h	0. 1977(2)	0.3954(4)	1/4	1.0*	0.5*
Al1	12k	0. 1605(8)	0.321(2)	0.9249(8)	1.11(1)	0.5*
Al2	6h	0.563(1)	0.125(3)	1/4	1.10(3)	0.5*
Al3	4f	1/3	2/3	0.022(2)	1.19(2)	0.5*
Al4	2b	0	0	1/4	1.04(4)	0.5*
Fe1	6g	1/2	0	0	1.07(1)	0.5*
Fe2	2a	0	0	0	1.10(1)	0.5*

*Fixed parameter.

Table 3
$U_3Fe_4Al_{12}$ interatomic distances (*d*) and number of nearest neighbours (NN)

	NN	Atoms	*d* (Å)		NN	Atoms	*d* (Å)
U(6h)	2	Al3(4f)	2.93(1)	Al1(12k)	1	Fe2(2a)	2.51(1)
	1	Al4(2b)	2.98(2)		2	Fe1(6g)	2.65(1)
	2	Al2(6h)	3.00(3)		1	Al3(4f)	2.76(1)
	2	Al1(12k)	3.05(1)		2	Al1(12k)	2.79(1)
	4	Al1(12k)	3.18(1)		2	Al2(6h)	2.79(2)
	4	Fe1(6g)	3.267(3)		1	Al4(2b)	2.91(2)
	2	U(6h)	3.54(1)		1	U(6h)	3.05(1)
					2	U(6h)	3.18(1)
Al2(6h)	2	Fe1(6g)	2.49(1)	Al3(4f)	3	Fe1(6g)	2.522(4)
	2	Al2(6h)	2.73(3)		3	Al1(12k)	2.76(1)
	4	Al1(12k)	2.79(2)		3	U(6h)	2.93(1)
	2	Al3(4f)	2.96(1)		3	Al2(6h)	2.96(1)
	2	U(6h)	3.00(3)				
Al4(2b)	2	Fe2(2a)	2.306(4)	Fe1(6g)	2	Al2(6h)	2.49(1)
	6	Al1(12k)	2.91(2)		2	Al3(4f)	2.522(4)
	3	U(6h)	2.98(2)		4	Al1(12k)	2.65(1)
					4	U(6h)	3.267(3)
Fe2(2a)	2	Al4(2b)	2.306(4)				
	6	Al1(12k)	2.51(1)				

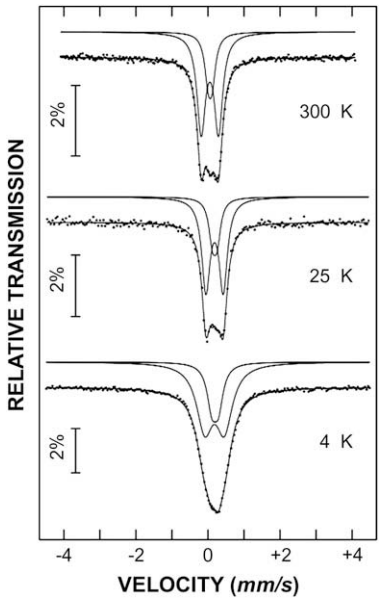

Fig. 3. Mössbauer spectra of $U_3Fe_{4+x}Al_{12-x}$ taken at different temperatures. The lines over the experimental points are the sum of two doublets, shown slightly shifted for clarity, (cf. Table 4).

The individual spectral features are less resolved at $T = 4$ K (Fig. 3). The spectrum may however be fitted with two doublets similar to those detected at higher temperatures. The estimated I and IS are in agreement with the higher temperature data but an increase in QS and Γ are observed.

5. Magnetic properties

As mentioned in Section 3, it was not possible to prepare a pure ternary $U_3Fe_{4+x}Al_{12-x}$ compound due to the large number of surrounding phases with high thermodynamic stability. For instance, the sample prepared with the initial stoichiometric ratio $U_3Fe_4Al_{12}$ (Fig 1) contained a small amount of UFe_xAl_{12-x} ($ThMn_{12}$-type) and showed ferromagnetic transitions at or below 150 K due to this spurious phase.

The knowledge of the ternary phase diagram, and thus of the different phase fields formation, allows to select the less undesirable impurities in samples for physical measurements. A sample with composition 1U:1Fe:3Al, located in the binary phase field $UAl_{2-x}Fe_x$ $(0.1 < x < 0.38)$ – $U_3Fe_{4+x}Al_{12-x}$ $(0 < x < 0.5)$ was prepared and contains, as expected, a small quantity of the $UAl_{2-x}Fe_x$ ($MgCu_2$ structure type) paramagnetic impurity [15] and $U_3Fe_{4+x}Al_{12-x}$, as the main phase. This sample was used for the magnetic characterization of $U_3Fe_{4+x}Al_{12-x}$: the magnetic features obtained were considered as arising from this compound, since the $MgCu_2$ structure type phase $UAl_{2-x}Fe_x$ present as impurity does not show any anomaly at low temperature [15].

Table 4
Estimated parameters from the Mössbauer spectra taken at 300 and 4 K

T (K)	Site	IS (mm/s)	QS (mm/s)	Γ (mm/s)	I
300	6g	0.16	0.48	0.28	74%
	2a	0.17	0.11	0.24	26%
25	6g	0.30	0.48	0.28	74%
	2a	0.30	0.13	0.24	26%
4	6g	0.30	0.54	0.55	74%
	2a	0.31	0.18	0.31	26%

IS, isomer shift relative to metallic α-Fe at 300 K; QS, quadrupole splitting; Γ, linewidths, I relative areas of the Fe contribution on each crystallographic site. Estimated errors for IS, QS, and Γ are ≤0.01 mm/s and for $I < 1\%$.

Fig. 4 shows the magnetization vs. temperature dependence measured in a field of 0.02 and 0.05 T, for the 1U:1Fe:3Al sample, free of any ferromagnetic impurity. The inset presents the inverse susceptibility up to room temperature, determined in a magnetic field of 2 T. The temperature variation of the susceptibility above 150 K obeys the Curie–Weiss law, $\chi = C/(T-\theta)$, with a paramagnetic Curie temperature $\theta_P = -25.5(1)$ K and a effective moment $\mu_{eff} = 3.54(1)\mu_B$ (calculated considering the 1U:1Fe:3Al formula). This last value is compatible with an uranium U^{3+} or U^{4+} configuration ($\mu_{eff}(U^{3+}) = 3.62\mu_B$ and $\mu_{eff}(U^{4+}) = 3.58\mu_B$, calculated for free uranium ions on the basis of the Russel–Saunders coupling). However, the free ion character of the uranium atoms in this compound is not expected. Indeed, most of the uranium effective moments observed in intermetallic compounds are in the $2–3\mu_B$ range, reflecting the participation in bonding of the 5f electrons and their hybridization with the valence states of neighbouring atoms in the crystal structure. Therefore, albeit an expected predominant uranium contribution, as discussed in detail below, the relatively high value of the effective moment points to a non-zero iron contribution to the total magnetic moment of $U_3Fe_{4+x}Al_{12-x}$. The nature of the crystal structure, with the iron atoms interacting with aluminium and without any direct exchange with uranium, is probably the reason for the presence of an iron magnetic moment in this compound, in spite of its small concentration. The $2.37\mu_B$ paramagnetic moment reported for the binary Fe_4Al_{13} compound [16] also suggests the possibility of an iron magnetic moment in $U_3Fe_{4+x}Al_{12-x}$. The negative Curie temperature implies that the dominant U–U interactions in $U_3Fe_{4+x}Al_{12-x}$ are antiferromagnetic-type. The specific arrangement of the uranium atoms, in a Kagomé network, and their predominant antiferromagnetic interactions are expected to generate frustrated magnetic correlations that could give rise to spin-glass behaviour. Such interesting property was already observed in the isostructural Co-based compound $U_3Co_{4+x}Al_{12-x}$ [7,8].

At low temperatures ($T < 10$ K) a pronounced magnetization feature is observed (Fig. 4), which points to a possible existence of a new magnetic state. The ZFC curve shows a pronounced peak, just below the irreversibility temperature ($T_{irr} = 7.7$ K, for $B = 0.02$ T). The position of this peak is strongly dependent on the magnetic field, its temperature being reduced with increasing field. AC-susceptibility measurements (Fig. 5) show that the temperature of this peak roughly coincides with a maximum (cusp) in χ' at $T = 7.9$ K. The magnetization curve as a function of the magnetic field, measured at $T = 1.8$ K, is presented in Fig. 6. The

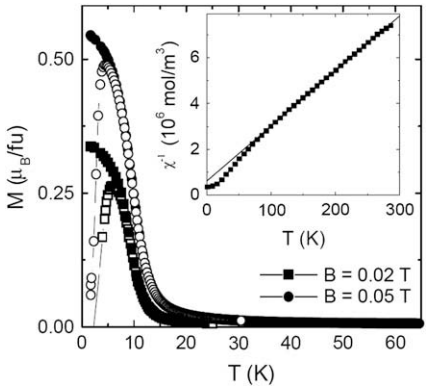

Fig. 4. Temperature dependence of the magnetization for a 1U:1Fe:3Al nominal composition sample, obtained at different applied fields (open symbols – ZFC; closed symbols – FC). The inset shows the temperature dependence of the inverse DC susceptibility obtained at 2 T.

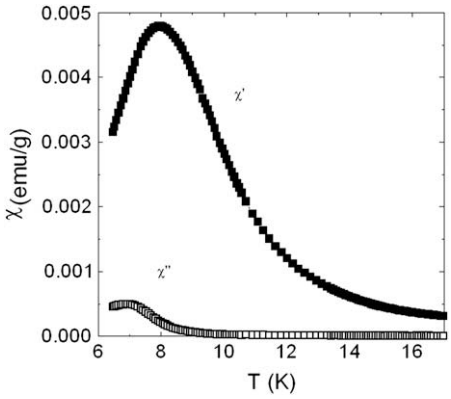

Fig. 5. Temperature dependence of the AC-susceptibility for the 1U:1Fe:3Al nominal composition sample (real part, χ'; imaginary part, χ'').

magnetization does not saturate up to the highest applied field of 7 T and hysteresis is observed in the low field part of the curve. Both these features point to a spin-glass state at low temperature. However, other phenomena, like the freezing of magnetic clusters in superparamagnets or domain effects in ferromagnets, can also give rise to similar behaviours.

The most conclusive and clear way to identify a spin-glass material, in which magnetic moments are frozen in a random configuration, is the frequency and field dependence of the cusp in χ'. The real and imaginary parts of the AC-susceptibility measured at different frequencies under a zero DC-magnetic field are shown in Fig. 7. The maximum in χ' shifts to lower temperatures and increases its height as the frequency of the excitation field decreases. This type of behaviour has been observed in many canonical spin-glass systems. The position of this cusp in χ' defines the freezing temperature, T_f, and is coincident with the temperature of the inflection point in χ''. The χ'' term is one order of magnitude smaller than χ' and above 9.5 K χ' is virtually independent of the frequency.

The effect of a superimposed DC-magnetic field on χ' close to the cusp is presented in Fig. 8. The AC-susceptibility shows a clear dependence on the magnetic field. The cusp position shifts to lower temperatures, with the corresponding maximum value strongly decreasing with the increasing magnetic field and almost vanishing for $B = 0.05$ T. This behaviour is explained in a spin-glass system by the fact that increasing the magnetic energy leads to the overcome of the energy barrier (or freezing temperature) between the

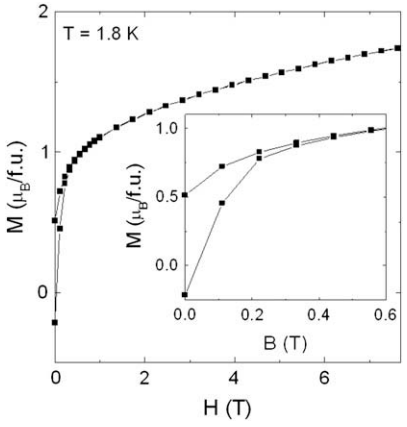

Fig. 6. Magnetization versus magnetic field for the 1U:1Fe:3Al nominal composition sample at 1.8 K; the inset shows in detail the low fields region.

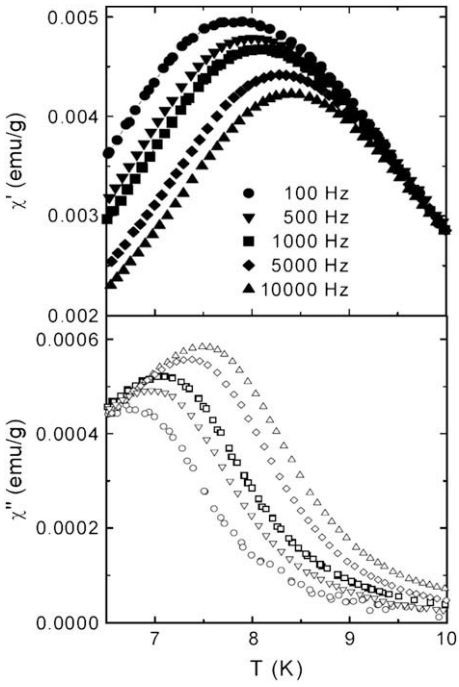

Fig. 7. Temperature dependence of the AC-susceptibility of the 1U:1Fe:3Al nominal composition sample at various frequencies and under an AC field of 10 Oe (real part, χ'; imaginary part, χ'').

possible magnetic moment positions, shifting and smoothing the cusp to lower values.

All the above observations are typical of the dynamic of spin-glass systems. However, and in order to further characterize the origin of the $U_3Fe_{4+x}Al_{12-x}$ magnetic behaviour, a subsequent analysis of the frequency dependence of the AC-susceptibility was performed. Depending on the strength of the interactions between the magnetic moments, T_f can be weakly (strong interactions) or strongly (weak interactions) dependent on the frequency. The initial frequency shift, $\Delta T_f/[T_f \Delta \log(\omega)]$, can give an idea on the origin of the above described magnetic behaviour. This quantity ranges from 0.004 to 0.025 for a spin-glass system (with strong interactions between the magnetic moments), while for superparamagnets it varies from 0.25 to 0.35 (with weak interactions between the clusters) [17]. The value calculated from experimental findings on $U_3Fe_{4+x}Al_{12-x}$ is ≈ 0.03, which is slightly higher but still consistent with the expected behaviour for a spin-glass system, considering that the sample contains a small amount of the paramagnetic phase $UAl_{2-x}Fe_x$.

There are two different interpretations for the magnetic moments' freezing, that leads to a spin-glass like behaviour: the first one considers a true equilibrium phase transition at a finite temperature (like in canonical spin-glass systems) [18]; the second one considers the existence of isolated magnetic clusters that freeze below a certain temperature (e.g. superparamagnets), being a non-equilibrium phenomenon [18]. In this latter case it is expected that the frequency dependence of the freezing temperature will follow the Arrhenius law:

$$\omega = \omega_0 \exp(-T_A/T_f) \quad (1)$$

where ω is the driving frequency of the AC-susceptibility measurement, $T_A = E_a/k_B$ and E_a is the characteristic energy of the activation barrier for the relaxation process between two easy orientations of the cluster. A fit of the experimental $1/T_f(\ln \omega)$ data yields the physically unreasonable $\omega_0 \approx 10^{33}$ Hz and

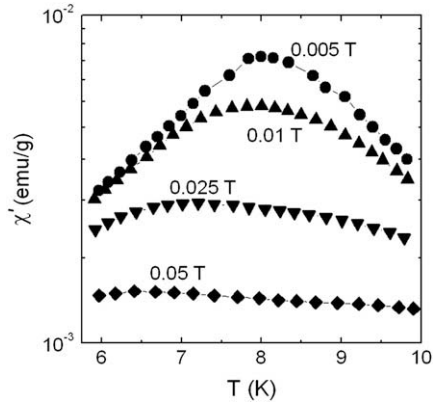

Fig. 8. Temperature dependence of the real part of the AC-susceptibility (χ') for the 1U:1Fe:3Al nominal composition sample under various DC fields.

$T_A = E_a/k_B = 535$ K values. However, in case of the slowing down with the decreasing temperature in a system composed of magnetically interacting particles, a better phenomenological description is given by the Vogel–Fulcher law:

$$\omega = \omega_0 \exp\left[-T_A/(T_f - T_0)\right] \quad (2)$$

where T_0 is a parameter that reflects the strength of the magnetic interactions. This last equation implies a linear dependence of T_f with $1/\ln(\omega_0/\omega)$ and has been often used to describe the slowing down of the relaxation found in spin glasses [19], with T_0 having the same order of magnitude of T_f. The Vogel–Fulcher plot for $U_3Fe_{4+x}Al_{12-x}$ is shown in Fig. 9. The three fitted parameters, $\omega_0 \approx 10^{13}$ Hz, $T_0 = 5.5$ K and $T_A = E_a/k_B = 54$ K, give reasonable values, which are consistent with a spin-glass behaviour for $U_3Fe_{4+x}Al_{12-x}$, considering that in this compound $T_f \approx 7.9$ K at 30 Hz.

A priori, an iron contribution to magnetization is not expected, in analogy with other iron-poor $U_xFe_yM_z$ (M = p element) intermetallics [5]. In fact, no magnetic hyperfine fields are detected in the Mössbauer spectra at 4 K which means that the dynamics of the fluctuations of the iron magnetic moments, μ_{Fe}, is too fast for the Mössbauer effect observation time. This implies that down to $T = 4$ K there is neither long-range magnetic ordering of the iron moments nor a freezing of their directions in a way typical of a spin-glass.

On the other hand, although the QS and Γ values are the same within experimental error between 300 and 25 K, small increases in QS and Γ are observed between 25 and 4 K (Table 4).

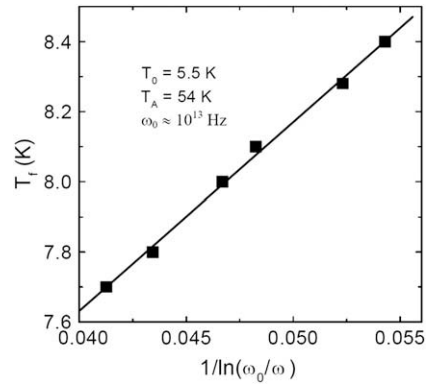

Fig. 9. Variation of the freezing temperature, T_f, with the frequency, ω, in a Vogel–Fulcher plot. The solid line represents the best fit of Eq. (2).

Considering the ^{57}Fe Mössbauer time window, the peak broadening could be explained by a certain slowing down of the μ_{Fe} dynamics to a frequency of about 10^8 s^{-1}. This slowing down is far from what would be observed if magnetic ordering or spin-glass freezing of μ_{Fe} occurred. It is rather similar to the effect attributed to polarization of the conduction electrons at the iron sites in RFe_2Si_2 compounds due to R, the rare-earth, magnetic ordering [20]. In contrast to RFe_2Si_2, however, the enhanced effective magnetic moment deduced for the present $U_3Fe_{4+x}Al_{12-x}$, suggests a non-zero μ_{Fe}. Furthermore the large U–Fe interatomic distances in $U_3Fe_{4+x}Al_{12-x}$ preclude a strong hybridization between these atoms that might lead to a negligible μ_{Fe}. The absence of long-range magnetic correlations between iron atoms in $U_3Fe_{4+x}Al_{12-x}$ seems to be rather due to the fact that all the atoms in the coordination polyhedron of iron are aluminium, while the Fe–Fe and Fe–U interatomic distances are significantly larger than the Fe–Al ones (Table 3). The Fe–Al distances are smaller than the sum of their metallic radii [14], pointing to a strong interaction between these two elements, and the Fe–Fe shortest interatomic distances are very large, hampering direct exchange magnetic interactions between them. In other intermetallics where the iron atoms are only surrounded by aluminium such as in the binary Fe_2Al_5 and Fe_3Al_{14} [21] or the ternary AFe_2Al_{10} (A = Y, U) [22] no freezing of the μ_{Fe} directions is observed down to 4 K and iron is paramagnetic as revealed by magnetic susceptibility data [16,22].

The anomalies detected by the magnetization data below 25 K may therefore be attributed to the uranium sublattice alone. The shortest U–U distances in $U_3Fe_{4+x}Al_{12-x}$ are above the Hill limit (3.4 Å) favoring the formation of uranium local moments. Moreover, the shortest U–Fe and U–Al interatomic distances are, respectively, much and slightly above the sum of their metallic radii [14], indicating small to medium hybridizations between the uranium atoms and their neighbours and, consequently, allowing the formation of sizeable uranium magnetic moments. The origin of the spin-glass like behaviour in $U_3Fe_{4+x}Al_{12-x}$ is most probably related to the topological frustration of these uranium moments as observed in the isostructural Co-based compound $U_3Co_{4+x}Al_{12-x}$ [7,8].

6. Conclusions

The $U_3Fe_{4+x}Al_{12-x}$ $(0 < x < 0.5)$ ternary uranium–iron–aluminium intermetallic was synthesized and found to crystallize in the hexagonal $Gd_3Ru_4Al_{12}$-type structure (S.G. $P6_3/mmc$). Its structure consists of U3Al4 layers alternating with FeAl layers along the hexagonal c axis, with the uranium atoms being located at the apexes of smaller and larger triangles, forming a distorted Kagomé net. The shortest U–U distances are slightly above the Hill critical distance, and the only iron atom belonging to the uranium coordination sphere is at a distance considerably above the sum of the uranium and iron metallic radii, pointing to a possible significant magnetic moment in both atoms.

The magnetic susceptibility follows a Curie–Weiss law above 150 K, with an effective moment of $\mu_{eff} = 3.54\mu_B$/f.u. (besides uranium, a small contribution from iron can be speculated) and a paramagnetic Curie temperature of $\theta_P = -25.5(1)$ K. At lower temperatures the magnetization and AC-susceptibility measurements revealed a spin-glass-type behaviour with a freezing temperature, $T_f = 7.9$ K. The magnitude of the frequency shift of the freezing temperature, 0.03, and the Vogel–Fulcher type dependence with $\omega_0 \approx 10^{13}$ Hz, $T_0 = 5.5$ K and $T_A = E_a/k_B = 54$ K are in agreement with a spin-glass picture. ^{57}Fe Mössbauer spectroscopy measurements indicate that the origin of the spin-glass behaviour is not related to the Fe sublattices and should therefore be

a consequence of the topological frustration of the uranium moments.

Acknowledgment

This work was partially supported by the exchange programme Pessoa (GRICES/EGIDE)-2007–2008, and by FCT, Portugal, under the contract no. PTDC/QUI/65369/2006. The authors also acknowledge fruitful discussions with Prof. L. Havela (Charles University, Prague, Czech Republic).

References

[1] Ramirez AP. In: Buschow KHJ, editor. Handbook of magnetic materials, vol. 13. Elsevier Science,; 2001. p. 423.
[2] Gonçalves AP, Noël H. Intermetallics 2005;13:580.
[3] Kuznietz M, Gonçalves AP, Waerenborgh JC, Almeida M, Cardoso C, Cruz MM, et al. Phys Rev B 1999;60:9494.
[4] Gonçalves AP, Pereira LCJ, Waerenborgh JC, Rojas DP, Almeida M, Havela L, et al. Physica B 2006;373:8.
[5] Noël H, Gonçalves AP, Waerenborgh JC. Intermetallics 2004;12:189.
[6] Gladyshevskii RE, Strusiecicz OR, Censual K, Parthé E. Acta Crystallogr, Sect B 1993;49:474.
[7] Tougait O, Troc R, Noël H. J Solid State Chem 2004;177:2053.
[8] Tougait O, Troc' R, Zaleski A, Noël H. Phil Mag 2007;87(7):1085–95.
[9] Nolze G, Kraus W. Powder cell for windows, version 2.2. Berlin: Federal Institute for Materials Research and Testing; 1999.
[10] Rodriguez-Carvajal J. FULLPROF, version 3.5d. LLB-JRC; 1998.
[11] Waerenborgh JC, Gonçalves AP, Almeida M. Solid State Commun 1999;110:369.
[12] Duong NP, Brück E, de Boer FR, Buschow KHJ. J Alloys Compd 2002;338:213–7.
[13] Niermann J, Jeitschko W. Z Anorg Allg Chem 2002;628:2549.
[14] Vainshtein BK, Fridkin VM, Indenbom VL. In: Cardona M, Fulde P, Queisser H-J, editors. Modern crystallography II, structure of crystals. Springer series in solid-state sciences, vol. 21. Berlin: Springer-Verlag; 1982. p. 71.
[15] Burzo E, Valeanu M. Appl Phys A 1984;35:79.
[16] Taylor MA. Proc Phys Soc Lond 1961;78:1244.
[17] Mydosh JA. Spin glasses: an experimental introduction. London: Taylor & Francis; 1993.
[18] Cardoso CA, Araújo-Moreira FM, Awana VPS, Takayama-Muromachi E, de Lima OF, Yamauchi H, et al. Phys Rev B 2003;67:020407.
[19] Ocko M, Drobac Dj, Park JG, Samardzija Z, Zadro K. J Phys Condens Matter 2003;15:4613.
[20] Noakes DR, Umarji AM, Shenoy GK. J Magn Magn Mater 1983;39:309.
[21] Preston RS, Gerlach R. Phys Rev B 1971;3(5):1519.
[22] Waerenborgh JC, Salamakha P, Sologub O, Sério S, Godinho M, Gonçalves AP, Almeida M. J Alloys Compd 2001;323:78.